Journal of Non-Crystalline Solids 560 (2021) 120726

Contents lists available at ScienceDirect

Journal of Non-Crystalline Solids

journal homepage: www.elsevier.com/locate/jnoncrysol

Effect of Mg content on electronic structure, optical and structural properties of amorphous ZnO nanoparticles: A DFTB study

Hasan Kurban [a,b], Sholeh Alaei [c], Mustafa Kurban [d,*]

[a] Computer Science Department, Indiana University, Bloomington, 47405 IN, USA
[b] Computer Engineering Department, Siirt University, 56100 Siirt, Turkey
[c] Department of Physics, Urmia Branch, Islamic Azad University, Urmia, Iran
[d] Department of Electrical and Electronics Engineering, Kırşehir Ahi Evran University, 40100 Kırşehir, Turkey

ARTICLE INFO

Keywords:
ZnO nanoparticle
Amorphous
Segregation phenomena
Electronic structure

ABSTRACT

In this work, we perform a theoretical analysis of structural, electronic, and optical properties of pure and Mg-doped amorphous ZnO nanoparticles (a-ZnO NPs) using DFTB method. Our results show that Zn atoms are more preferential for Mg atoms than for O atoms because the number of Mg—Zn bonds is greater than that of Mg—O. The rise in the content of Mg in a-ZnO NPs leads to an increase of Mg–Zn and Mg—O interactions. Mg atoms prefer to locate near the center of a-ZnO NP, but Zn and O atoms nearly preserve their positions which is compatible with radial distribution function peaks. The orbital energies display a decrease in the energy gap from 3.592 to 3.546 eV while increasing Mg content. The LUMO level is also significantly shifted to higher energies. The results also reveal that the performance of pure a-ZnO NP can be enhanced with a subsequent increase in Mg content.

1. Introduction

Among II–VI group of semiconductors, Zinc oxide (ZnO) has attracted great scrutiny due to its unique electronic structure, chemical and optical properties as well as high abundance in nature and non-toxicity [1–3]. Due to its desirable chemical properties according to stability and catalytic activity, ZnO has been used as a good candidate in many areas including solar cells, gas sensors, optoelectronics, and ultraviolet light-emitting/detecting devices [3–5]. In addition to bulk ZnO, more specifically, its nanostructures such as nanoparticles (NPs), nanorods, nanotubes, nanowires, nanobelts, nanosprings, nanosaws, etc., have been grown using various methods [6–11]. Among them, significant attention has been paid to ZnO NPs due to their fascinating properties, being widely studied in various fields as photodetectors [12], energetic materials [13], and biomedical agents [14].

Recent studies show that it is possible to get better or desirable features of materials by doping an atom or changing their structural properties under high temperature or pressure, especially at nanolevel [15–17]. Herein, many efforts have been carried out on Al, Ca, Cu, Fe, Co, Sn, Mn, Ga, Li and Mg-doped ZnO NPs to enhance the structural and optoelectronic properties of pure ZnO NPs [18–25]. The obtained results from the literature show that the use of doped ZnO NPs allows improving the sensitivity, electrocatalyst and photocatalytic properties, current efficiency of light-emitting diodes and antibacterial reducing the spread of bacterial infections. On the other hand, the amorphous transparent oxide materials, especially ionic amorphous oxide ones, have vast use in device technology. Among these oxide semiconductors, amorphous ZnO (a-ZnO) has high electron mobility (~ 5-40 cm^2 /V s) making it a suitable candidate for the application of thin-film transistors. In comparison to the crystalline form of ZnO, the amorphous counterpart possesses some advantages such as efficient optical properties, lower cost, and easier methods to produce a large sheet of this kind of material at low temperatures [26,27]. Besides, the energy gap of a-ZnO is found as 1.60 eV (experimental) [28] and 0.74 eV (theoretical) [29], which are considerable smaller than its crystal form (3.37 eV) [30]. As can be seen from the literature, the doping process and amorphous lead to some significant advantages over the pure and crystalline ZnO.

In the present paper, the influences of Mg content on electronic structure, optical and structural properties of a-ZnO NPs have been performed by the density-functional tight-binding (DFTB) approach. When compared with relevant studies mentioned above, the novelty and advantages of this study are to investigate doping Mg atoms on a-ZnO NPs for the first time. In this perspective, we have carried out the variation of the number of bonds of binary Mg—Mg, Mg—O, Mg—Zn,

* Corresponding author.
E-mail addresses: mkurbanphys@gmail.com, mkurban@ahievran.edu.tr (M. Kurban).

https://doi.org/10.1016/j.jnoncrysol.2021.120726
Received 22 December 2020; Received in revised form 3 February 2021; Accepted 4 February 2021
Available online 12 February 2021

Zn—Zn and O—Zn interactions, segregation phenomena of Mg, Zn and O atoms, radial distribution function (RDF), the density of states (DOS), orbital energies (HOMO, LUMO and HOMO-LUMO energy gap), and refractive index as a function of Mg concentration.

2. The method of calculations

We used the DFTB+ code [31], which is an implementation of DFTB method, with the 3ob/3ob-3-1 ,[32,33] set of Slater Koster parameters. ZnO NP was carved from a wurtzite bulk ZnO 60 × 60 × 60 supercell. To create a spherical NP model with desirable radius, which is chosen as 0.9 nm in this study, the atoms within the spherical area are only considered, but the other atoms are removed from the supercell. The crystalline ZnO needs to grow stands at high temperature (773–1073 K) [34], which is a significant disadvantage against a-ZnO, which can be prepared at low temperature, even at room temperature [30]. In this study, the ZnO NP was first melted by heating it to 2300 K almost corresponding to experimental melting point (2247 K) of ZnO [35], within the NVT ensemble in the frame of molecular dynamics (MD) simulations. The time step of MD was chosen as 1 fs. Then, the melt structure was cooled to 300 K to obtain an amorphous structure.

The number of bonds (n_{ij}) is an important parameter for NPs and used to differentiate the degree of packing in general. The n_{ij} [36] is expressed by

$$n_{ij} = \sum_{i<j} \delta_{ij} \tag{1}$$

where $\delta_{ij} = \begin{cases} 1, & r_{ij} \le 1.2 r_{ij}^{(0)} \\ 0, & r_{ij} > 1.2 r_{ij}^{(0)} \end{cases}$ i,j = Mg, Zn or O, r_{ij} is the distance between atom i and j and $r_{ij}^{(0)}$ is a nearest neighbor criterion derived by fitting the binary data of . We perform, in this study, the atomic distribution of Mg, Zn and O atoms in the studied pure and Mg-doped a-ZnO NPs using n_{ij}.

It is one of the major problems of some materials [37] to set up a stable structure for providing materials with high-efficiency. It is known that the distribution of atoms in crystalline materials is, homogeneous [38], but not for amorphous materials. In this perspective, we analyzed the order parameter (R_{T_i}) which explores the distribution of the different types of atoms [39] to find the stable structure in NPs. Let n_{T_i} be the number T_i type atoms in the ternary *ABC* NPs, r_i the distance of the atoms to the coordinate center of the NP, then R_{T_i}, the average distance of a type T_i atoms in accordance with the center of a NP, is calculated as follows:

$$R_{T_i} = \frac{1}{n_{T_i}} \sum_{i=1}^{n_{T_i}} r_i \tag{2}$$

An $\in$ distance from center of NP to a reference point is defined to show the location of atoms; if $R_{T_i} < \in_{min}$ (a "small" value), the T_i type atoms are at the center, and if $R_{T_i} > \in_{max}$ (a "large" value), the T_i type atoms are at the surface region of NP. If neither is true, *i.e.*, if $\in_{min} \le R_{T_i} \le \in_{max}$ (a "medium" value), a well-mixed NP.

3. Results and discussion

Fig. 1 shows the optimized structures of pure and some of Mg-doped a-ZnO NPs with various concentrations of Mg. In Fig. 2, the log of the number of bonds shows the variation of the number of bonds of binary interactions in the Mg-doped ZnO NPs as a function of Mg concentration. The number of Mg—Mg bonds increases with an increase in Mg doping concentration which authenticates the little loss in the crystallinity originating from distortion of the lattice. Considering Fig. 2, the number of Mg—O and Mg—Zn bonds increases with a raise in the content of Mg atoms, while the bond numbers of Zn—Zn and O—Zn reduce. In other words, the average number of Zn—Zn and Zn—O bonds was calculated less as the number of dopants increases. Besides, the bond numbers of Mg—Z and Mg—O are relatively greater than other bonds. This holds out that O and Zn atoms tend to make more bonds with Mg doping, but Zn atoms have more tendency to bond with Mg than O atoms. Comparing all possible number of bonds, the increase in Mg doping leads to the sharp increase in the number of O and Zn bonds. The reduction of the number of Zn-Zn and O-Zn bonds is not as sharp as the increment of Mg—Zn and Mg—O bond numbers, i.e., the change in the number of the

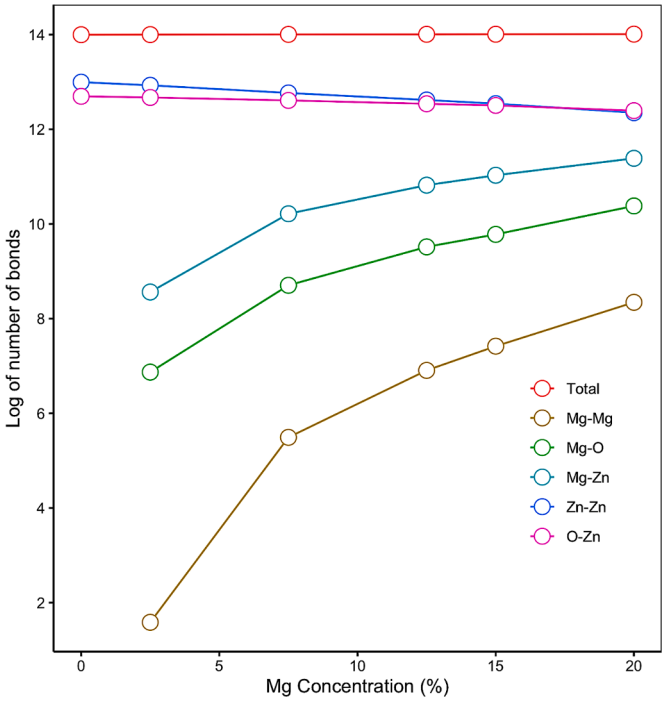

Fig. 2. Variation of number of bonds of binary Mg—Mg, Mg—O, Mg—Zn, Zn-Zn and O—Zn interactions as a function of Mg concentration.

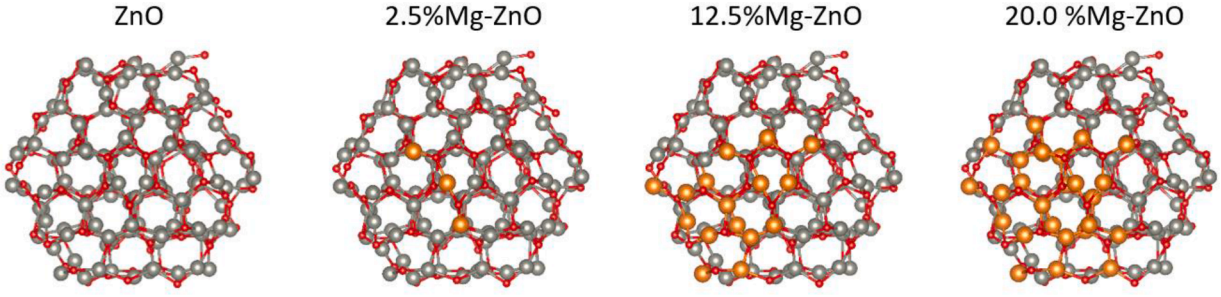

Fig. 1. Optimized structures of pure and Mg-doped amorphous ZnO nanoparticles (Mg is orange, Zn is gray, and O is red). (For interpretation of the references to color in this figure legend, the reader is referred to the web version of this article.).

first ones is not significant as the latter bond numbers.

The order parameter (R) is one of the factors used to understand the distribution of atoms in a material. Thus, according to the R, the stable structure of NPs can be analyzed. The definition of the R was presented in our previous paper [40]. The R is employed for determining the segregation phenomena of atoms in Mg-doped a-ZnO NPs. As it is displayed in Fig. 3, with the increase of doping concentration, Mg atoms prefer to locate near the center of NP and try to indwell most portion of it. However, Zn and O atoms is completely opposite to Mg atoms. The Zn and O atoms have tendency to preserve their positions in the Mg-doped a-ZnO NPs and make their effort not to shift their locations. In addition to this trend, on the other hand, as Mg concentration rises, the dopant ions may replace Zn ions in the host lattice. In addition, it is observed that Mg atoms tend to place near the surface in a-ZnO NPs. The radius of Mg^{2+} ions is smaller than Zn^{2+} ion ones, thus, some of Mg^{+2} ions may substitute Zn^{2+} ions. The R for Mg exhibits a slight drop as the Mg concentration increases and varies widely with an increase in the concentration of Mg atoms, while the R remains nearly constant for O atoms. But for Zn atoms, the R exhibits a gradual decrease, caused by the presence of 5-10% of Mg atoms within a-ZnO NPs, then returns to the previous value. In the literature, it is reported that incorporation of dopant atoms affects the lattice structure of the host materials [41]. Moreover, the basic structure of a-ZnO NPs like crystalline ones is not modified and retains their original structure.

Using the obtained results, we explore the influence of doping concentration of Mg atoms on the formation of a stable structure a-ZnO NPs. Calculating the Radial Distribution Function (RDF) of the bond lengths between the constituent atoms is one of the techniques used to quantify the lack of long-range crystalline order to be the defining feature of amorphous structures. The RDF can be used to verify the structure evolution of a-ZnO NPs in the presence of different concentrations of Mg atoms. The shape and location of the RDF peaks also allow determining a model of the atomic structure of NPs and estimating the disorder and amorphous form.

Fig. 4-up presents the RDF for Zn-Zn and O-O binary interactions in the pure a-ZnO NP. All RDF calculations are done for each optimized atomic pair of a-ZnO NP. The results show that there is one outstanding peak with values of 6.2 and 4.8 for Zn and O atoms with a distance of 1.7 Å and 1.9 Å corresponding to pure ZnO, respectively. Therefore, Zn—Zn interactions possess higher and sharper peak distribution than O—O interactions. However, O atoms have larger RDF than Zn atoms, i.e., O atoms placed in inner shells near to the center of a-ZnO NP. The positions of these peaks are in line with experimental and theoretical peaks

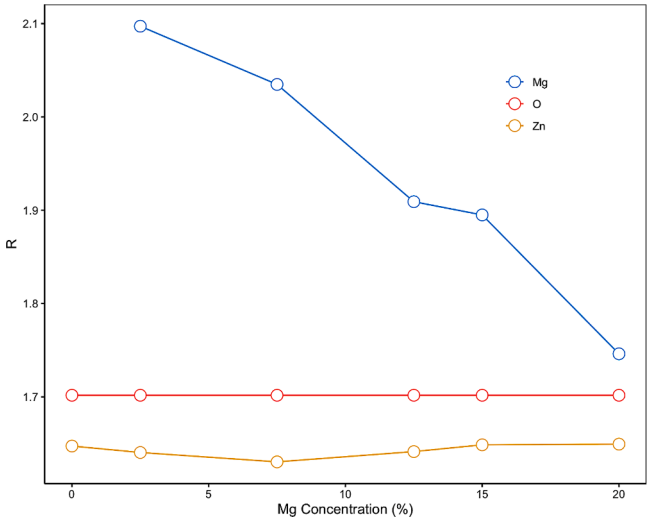

Fig. 3. Mg concentration dependence of the order parameter of Mg, Zn and O atoms in pure and Mg-doped amorphous ZnO nanoparticles.

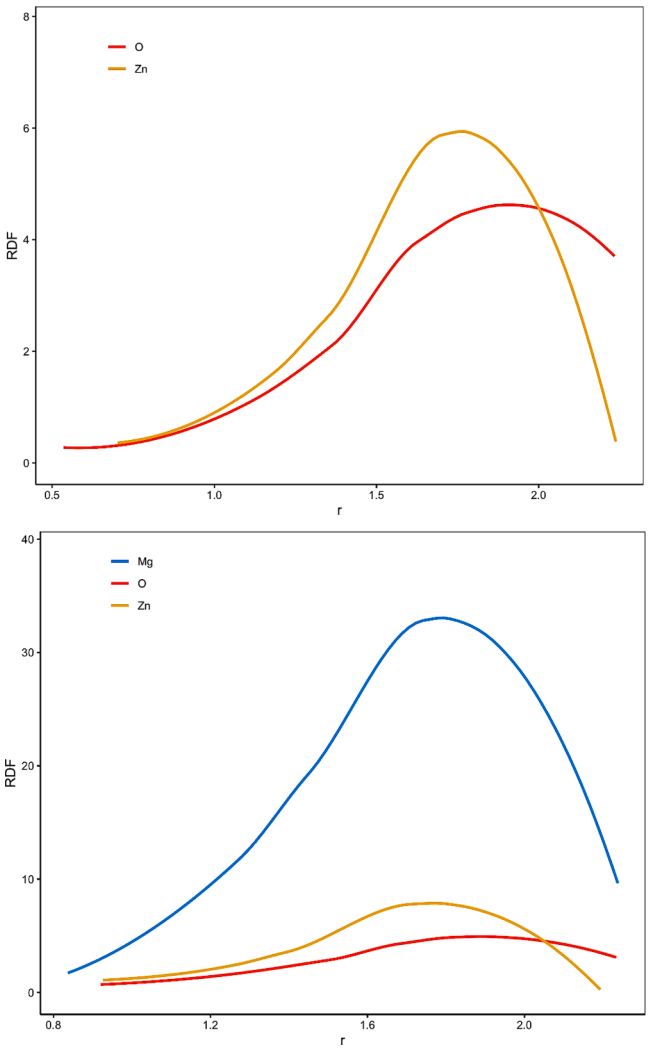

Fig. 4. Radial distribution function of pure (up) and 20% Mg-doped amorphous ZnO (down) nanoparticles.

in the literature which has reported around 2 Å [42,43]. It is comprehended that the ZnO bulk character is preserved in the amorphous sample, as well. This behavior has also been observed in other amorphous oxides [42,43]. Furthermore, the maximum point of RDF peaks of Zn and O interactions nearly compatible with those for crystalline ZnO [44].

We also observe that, on the one hand, in Mg-doped a-NPs, the RDF of Zn and O atoms are similar, whereas it is also completely different in peak height and position for Mg (shown in Fig. 4-down). Thus, dopant Mg influences the RDF values when compared to pure a-ZnO NP. For 20% Mg-doped a-ZnO NP, the RDF values for Mg has moved to higher values in comparison to values of Zn and O peaks. The distributions of Mg atoms are also wider than in the case of Zn and O atoms. This confirms that the Mg atoms tend to locate near the surface of Mg-doped a-ZnO NP. The maximum RDF peak of Mg atoms is also greater than that of Zn and O. The RDF of this peak which is around 34 at a radius of 1.8 Å is related to the maximum concentration of Mg doping. Moreover, the Zn and O peaks are not perceptibly affected by the presence of Mg atoms as dopants, there is only a slight decrease in the RDF peaks of mentioned atoms. This shows that Zn and O atoms start to fluctuate from their equilibrium positions swiftly, so the peak positions change very slightly.

To get better insight on the electronic structure of pure and Mg-doped a-ZnO NPs, the total density of states with a wide range of Mg doping concentrations is performed as shown in Fig. 5. The DOS

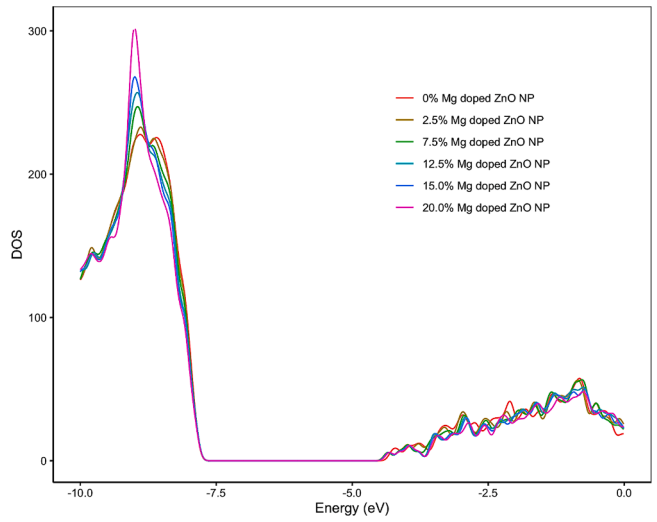

Fig. 5. The total density of states (DOS) of pure and Mg-doped amorphous ZnO nanoparticles.

analyses indicate that the greatest contribution results from 20% and 15% Mg-doped a-ZnO NPs. The main reason of fluctuations in the DOS is the concentration percentage of doping with Mg into a-ZnO NPs. Experimental findings show that ZnO NPs possess the energy gaps of approximately 3.5 eV [45]. The study show that the energy gap is remarkably affected by some factors such as phase structure, size of the structure, temperature. It can be evidently noticed that the energy gaps of Mg-doped ZnO NPs decrease significantly compared with pure ZnO and thus both the valence band (VB) to the conduction band (CB) shift toward the low-energy region. It is interesting to note that the increase in the CB is greater than that of the VB.

Investigations about the energy gap modulation with Mg content and their relations do not follow a similar trend for crystalline and amorphous ZnO. In this regard, more studies about the role of various factors along with doping concentration on widening or narrowing of the energy gap of a-ZnO NPs is needed. In Fig. 6, the HOMO-LUMO energy gap of pure and Mg-doped a-ZnO NPs as a function of Mg concentration are presented. Highest occupied molecular orbital (HOMO) as electron donors and lowest unoccupied molecular orbital (LUMO) as electron acceptors are important parameters to determine the reactivity of NPs. The energy difference between HOMO and LUMO orbits is called as the

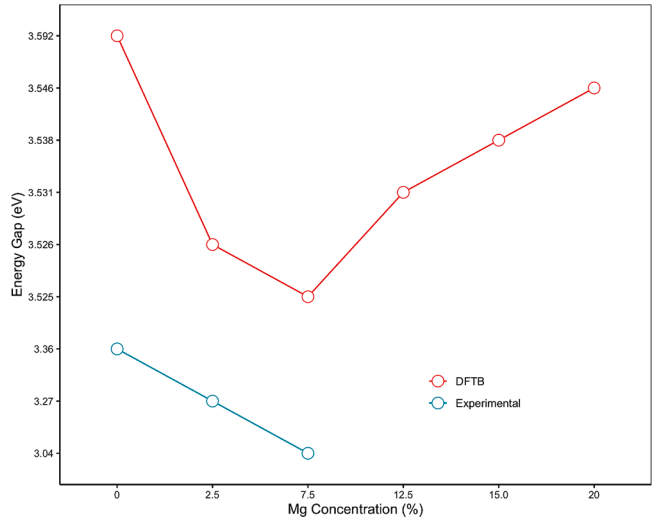

Fig. 6. The HOMO-LUMO energy gap of pure and Mg-doped amorphous ZnO nanoparticles as a function of Mg concentration.

energy gap which is important stability for the structure.

The predicted results for the HOMO-LUMO gap for the ZnO NPs from DFTB calculations and experimental are compared in Fig. 6. For pure ZnO NPs, we find that the predicted energy gap value obtained from calculations equals 3.592 eV which is the highest HOMO-LUMO gap. The calculated result is compatible with experimental data of 3.36 eV [24]. Considering the effect of Mg doping concentration, we observe that the HOMO-LUMO gap drops rapidly to a value of 3.526 eV in the case of 2.5% Mg-doped a-ZnO NP. The lowest HOMO-LUMO gap for the doped ZnO NPs results in 7.5% Mg concentration with the value of 3.525 eV (the electronic gap) from DFTB and its experimental value is 3.04 eV (the optical gap). The differences between theory and experiment are expected results because the electronic energy gap is larger than that of optical gap. Furthermore, the trend just documented is not obeyed for Mg concentrations more than 7.5%, i.e., for 12.5% Mg doping and more, the HOMO-LUMO gap increases as dopant concentration rises. From Fig. 6, the energy gaps correlate with a higher fraction of Mg doping, i.e., 12.5, 15 and 20% are 3.5310 eV, 3.5380 eV and 3.546 eV, respectively. However, in the literature, there is no study on Mg doping concentration more than 7.5% for ZnO NP.

A similar trend in the bandgap upon doping was also observed for Ag-doped ZnO [46], but it is observed some fluctuations for Cr and Mg-doped ZnO. Chang et al. reported that the decrease in the optical bandgap of ZnO NPs with dopant Cr could eventuate in the formation of defects and higher flow of electrons from the VB to CB of ZnO material, so caused augmentation of the electronic conductivity of the material [47]. Thus, due to the presence of dopant, ZnO NPs indicate a bandgap significantly smaller than that of its crystalline structure. It is very likely that similar effects are observed in the present study. We find out that increasing of Mg doping concentration up to 20% eventuates in narrower the energy gap in comparison with pure material but wider than minor Mg doping concentration. Many other studies show that the content of Mg atoms influences bandgap of crystalline ZnO nanostructure and reported controversial results about its effect on the fluctuations of bandgap. It is noteworthy to mention that, to the best of our knowledge, there is no theoretical nor experimental report on the Mg doping concentration augmentation effect on a-ZnO. Thus, it can be concluded that Mg doping may provide an efficient way to modulate the energy gap in a-ZnO.

To obtain a broader perspective on the effect of Mg content, the HOMO and LUMO energy levels of pure and Mg-doped a-ZnO NPs are presented in Fig. 7. We observe that the HOMO and LUMO energy levels are -7.855 eV and -4.263 eV respectively, generating an energy gap value of about 3.592 eV for pure ZnO NPs. After doping 2.5% Mg atoms on a-ZnO NPs, the HOMO and LUMO energies reduce values of -7.874 eV and -4.348 eV, respectively. The energy band gap of 2.5% doped a-ZnO NPs significantly decreases from 3.592 eV to 3.526 eV upon Mg doping. As seen in Fig. 7, after the increase in the Mg content, the LUMO level is significantly shifted to higher energies, while the trend is different in HOMO energy level. It is obvious that in the case of 7.5% Mg-doped ZnO, the HOMO increases from -7.874 eV to -7.869 eV which agrees with LUMO behavior. However, the trend is not similar for 12.5 and 15% doping concentration, i.e., HOMO decreases to -7.870 eV. For increasing Mg doping concentration, repeatedly, a rise in HOMO level to -7.867 eV occurs and thus the energy gap is predicted as 3.546 eV. The energy gap values of Mg-doped a-ZnO NPs were decreased with doping of Mg, and the narrower band gap belongs to 7.5% concentration of Mg doping. We noticed that the increase in Mg doping content results in fluctuations in the energy gap, HOMO and LUMO. Many studies have been reported on the fact of the narrow and decreased energy gap for doped crystalline ZnO with Mg, Ag, In and Ni [48–50].

According to the previous studies, different dopant atoms can adjust the energy gap of ZnO, so it helps to make UV photodetectors and photoconductive detectors in different UV regimes [51,52]. In this regard, there has been a great interest in high optical refractive index n and larger energy gap because of the applications of ZnO material in

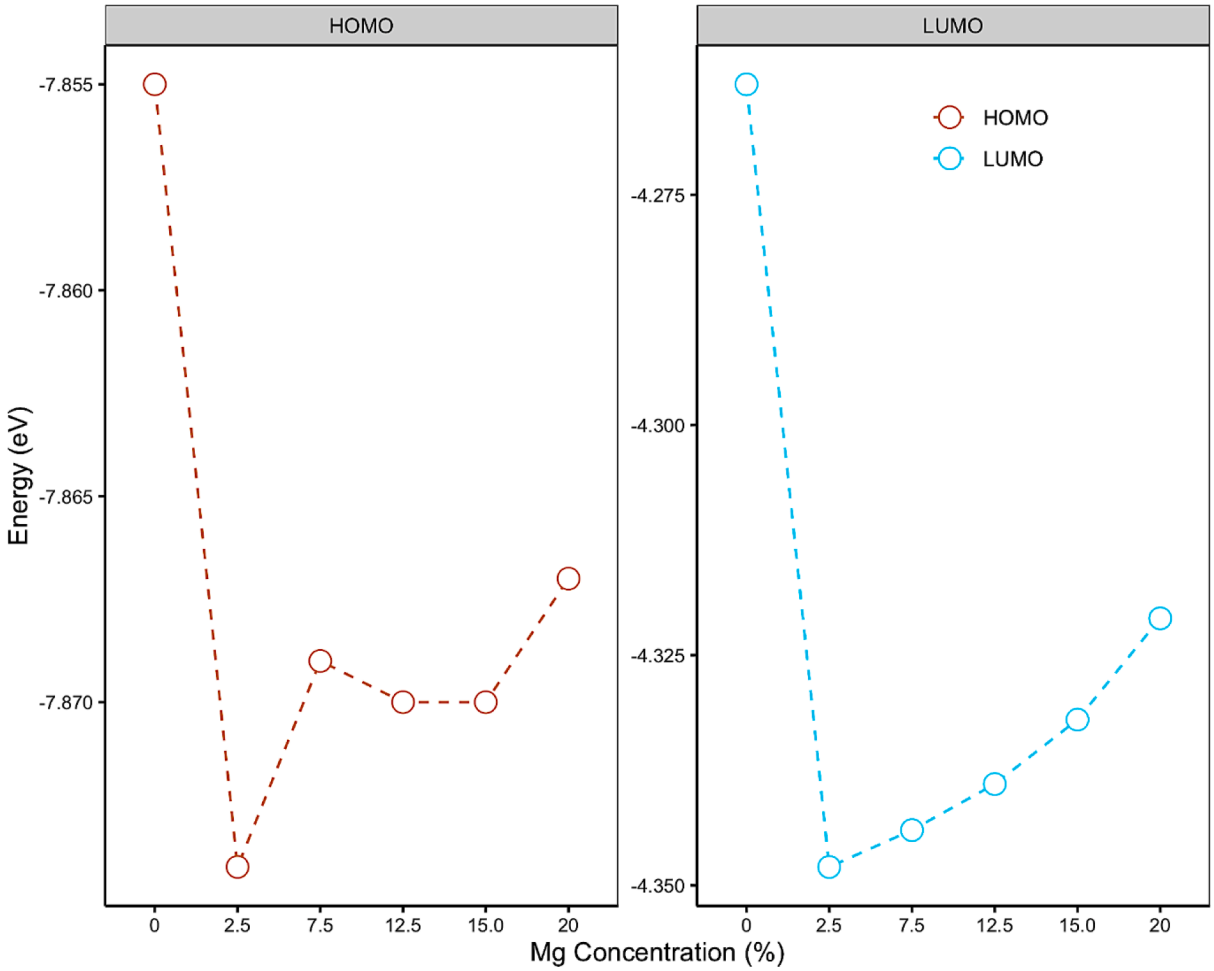

Fig. 7. HOMO and LUMO energy levels of pure and Mg-doped amorphous ZnO nanoparticles as a function of Mg concentration.

optoelectronic and sensor industries. The refractive index, *n* is, on the other hand, one of important parameters for optical materials and applications.

The calculated *n* of pure and Mg-doped a-ZnO NPs are displayed in Fig. 8. The obtained *n* values are calculated as based on Moss, Ravindra, Hervé-Vandamme and Kumar-Singh relations. Considering Ravindra model, the *n* is in the range of 1.856 - 1.885 and it increases from 1.856 for pure ZnO to 1.897 and 1.898 for 2.5 and 7.5% Mg doping concentration, respectively. For more Mg doping concentration, little decrease is found for *n* values, but, generally, it can be concluded that Mg doping increases the *n*. Moreover, the *n* of pure a-ZnO goes up with an increase in Mg content for both Moss and Kumar models, and it is placed in the range of 2.229- 2.238 for Kumar relation and 2.267 to 2.275 for Moss relation. The *n* values obtained from Hervé-Vandamme relation are higher than of other relations. It is the highest for 7.5 % Mg doping concentration with the value of 2.885. All four NP models present the same pattern between Mg doping concentration and the *n* and thus give similar results. To improve the performance of optical devices, optical sensors and optical interference filters, there is a need not only for the high *n* but also for wide energy gap materials. Besides, a higher Mg content (7.5% or more) on ZnO NPs gives rise to an increase in the *n* value.

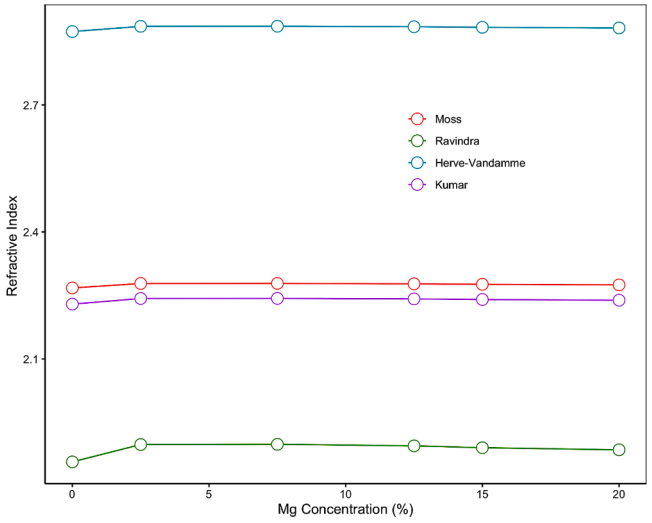

Fig. 8. Refractive index of pure and Mg-doped amorphous ZnO nanoparticles as a function of Mg concentration.

4. Conclusion

In the present study, the effect of Mg content on electronic structure, optical and structural properties of a-ZnO NPs, for the first time, has been carried out by the DFTB approach. We examine the number of bonds, order parameter, and RDF of two-body Mg, Zn and O interactions. Our results show that Mg atoms prefer to bond with Zn and O atoms, so the number of Mg—O and Mg—Zn bonds increases with a raise in the content of Mg atoms while the number of Zn—Zn and O—Zn bonds reduces. Also, Mg atoms tend to interact with Zn atoms more than O atoms. The segregation of Mg, Zn and O atoms indicates that Mg atoms

tend to locate at the center, while Zn and O atoms keep nearly their locations. The energy gap of pure a-ZnO NPs is reduced from 3.59 eV to 3.54 eV with the dopant Mg atoms due to the considerable change in the LUMO level. The trend of the energy gap is also consistent with experimental results. Finally, a higher Mg content in the ZnO NPs gives rise to an increase in the refractive index. Overall, Mg-doped a-ZnO NPs have more desirable properties than that of the pure ZnO, so they can be preferred as a promising material for optoelectronic applications.

CRediT authorship contribution statement

Hasan Kurban: Software, Visualization, Resources, Formal analysis, Data curation, Writing - review & editing. **Sholeh Alaei:** Investigation, Writing - original draft. **Mustafa Kurban:** Supervision, Project administration, Investigation, Conceptualization, Writing - original draft, Writing - review & editing, Data curation, Validation, Formal analysis, Software.

Declaration of Competing Interest

The authors declare that they have no known competing financial interests or personal relationships that could have appeared to influence the work reported in this paper.

References

[1] D.G. Thomas, The exciton spectrum of zinc oxide, J. Phys. Chem. Solids 15 (1-2) (1960 Aug 1) 86–96.
[2] M. Laurenti, S. Stassi, M. Lorenzoni, M. Fontana, G. Canavese, V. Cauda, C.F. Pirri, Evaluation of the piezoelectric properties and voltage generation of flexible zinc oxide thin films, Nanotechnology 26 (21) (2015 May 6), 215704.
[3] J.F. Wager, B. Yeh, R.L. Hoffman, D.A. Keszler, An amorphous oxide semiconductor thin-film transistor route to oxide electronics, Curr. Opin. Solid State Mater. Sci. 18 (2) (2014 Apr 1) 53–61.
[4] M. Laurenti, G. Canavese, S. Stassi, M. Fontana, M. Castellino, C.F. Pirri, V. Cauda, A porous nanobranched structure: an effective way to improve piezoelectricity in sputtered ZnO thin films, RSC Adv. 6 (80) (2016) 76996–77004.
[5] J. Liu, M.V. Fernández-Serra, P.B. Allen, First-principles study of pyroelectricity in GaN and ZnO, Phys. Rev. B 93 (8) (2016 Feb 9), 081205.
[6] R.Q. Song, A.W. Xu, B. Deng, Q. Li, G.Y. Chen, From layered basic zinc acetate nanobelts to hierarchical zinc oxide nanostructures and porous zinc oxide nanobelts, Adv. Funct. Mater. 17 (2) (2007 Jan 22) 296–306.
[7] Y. Liu, X. Wang, L. Fu, D. Zhu, Tower-like structure of ZnO nanocolumns, Chem. Commun. (11) (2003) 1304–1305.
[8] J. Zhang, L. Sun, C. Liao, C. Yan, A simple route towards tubular ZnO, Chem. Commun. (3) (2002) 262–263.
[9] X.Y. Kong, Y. Ding, R. Yang, Z.L. Wang, Single-crystal nanorings formed by epitaxial self-coiling of polar nanobelts, Science 303 (5662) (2004 Feb 27) 1348–1351.
[10] X. Zhong, W. Knoll, Morphology-controlled large-scale synthesis of ZnO nanocrystals from bulk ZnO, Chem. Commun. (9) (2005) 1158–1160.
[11] S. Polarz, A.V. Orlov, F. Schüth, A.H. Lu, Preparation of high-surface-area zinc oxide with ordered porosity, different pore sizes, and nanocrystalline walls, Chem.-a Eur. J. 13 (2) (2007) 592–597.
[12] S-P. Chang, K-J. Chen, Zinc oxide NP photodetector, J. Nanomater. 2012 (2012) 1–5.
[13] A.A. Barzinjy, S. Mustafa, H.H.J. Ismael, Characterization of ZnO NPs prepared from green synthesis using Euphorbia Petiolata leaves, EAJSE 4 (2019) 74–83.
[14] Y. Zhang, T.R. Nayak, H. Hong, W. Cai, Biomedical applications of zinc oxide nanomaterials, Curr. Mol. Med. 13 (10) (2013) 1633–1645.
[15] A.Ö. Karacaoğlan, M. Durandurdu, A first principles study of amorphous and crystalline silicon tetraboride, Mater. Chem. Phys. 258 (2021), 123928.
[16] M. Kurban, Tunable electronic structure and structural transition of GaAs clusters at high pressure and temperature, J. Alloys Compd. 791 (2019) 1159–1166.
[17] M. Kurban, Electronic structure, optical and structural properties of Si, Ni, B and N-doped a carbon nanotube: DFT study, Optik 172 (2018) 295–301.
[18] M. Hjiri, et al., Doped-ZnO nanoparticles for selective gas sensors, J. Mater. Sci. Mater. Electron. 28 (13) (2017) 9667–9674.
[19] S. Kumaresan, et al., Synthesis and systematic investigations of Al and Cu-doped ZnO nanoparticles and its structural, optical and photo-catalytic properties, J. Mater. Sci. Mater. Electron. 28 (13) (2017) 9199–9205.
[20] S. Das, et al., Disinfection of multidrug resistant Escherichia coli by solar-photocatalysis using Fe-doped ZnO nanoparticles, Sci. Rep. 7 (1) (2017) 1–14.
[21] Y. Sun, et al., Ultrafine Co-doped ZnO nanoparticles on reduced graphene oxide as an efficient electrocatalyst for oxygen reduction reaction, Electrochim. Acta 224 (2017) 561–570.
[22] T. Jan, J. Iqbal, et al., Sn doping induced enhancement in the activity of ZnO nanostructures against antibiotic resistant S. aureus bacteria, Int. J. Nanomed. 8 (2013) 3679.
[23] T. Rezkallah, et al., Investigation of the electronic and magnetic properties of Mn doped ZnO using the FP-LAPW method, Chin. J. Phys. 55 (4) (2017) 1432–1440.
[24] K. Sadaiyandi, et al., Influence of Mg doping on ZnO nanoparticles for enhanced photocatalytic evaluation and antibacterial analysis, Nanoscale Res. Lett. 13 (1) (2018) 1–13.
[25] A. Alexandrov, et al., Al-, Ga-, Mg-, or Li-doped zinc oxide nanoparticles as electron transport layers for quantum dot light-emitting diodes, Sci. Rep. 10 (1) (2020) 1–11.
[26] J. Robertson, Physics of amorphous conducting oxides, J. Non Cryst. Solids 354 (19-25) (2008 May 1) 2791–2795.
[27] H. Hosono, Ionic amorphous oxide semiconductors: Material design, carrier transport, and device application, J. Non. Cryst. Solids 352 (9-20) (2006 Jun 15) 851–858.
[28] D. Schmeißer, et al., Electronic structure of amorphous ZnO films, Phys. Status Solidi 11 (9-10) (2014) 1476–1480.
[29] D. Tahaoğlu, M. Durandurdu, Permanent densification of amorphous zinc oxide under pressure: a first principles study, J. Non. Cryst. Solids 481 (2018) 27–32.
[30] J.M. Khoshman, M.E. Kordesch, Optical constants and band edge of amorphous zinc oxide thin films, Thin Solid Films 515 (18) (2007) 7393–7399.
[31] B. Aradi, B. Hourahine, T. Frauenheim, DFTB+, a sparse matrix-based implementation of the DFTB method, J. Phys. Chem. A 111 (26) (2007 Jul 5) 5678–5684.
[32] M. Gaus, A. Goez, M. Elstner, Parametrization and benchmark of DFTB3 for organic molecules, J. Chem. Theory Comput. 9 (1) (2013 Jan 8) 338–354.
[33] M. Kubillus, T. Kubar, M. Gaus, J. Rezac, M. Elstner, Parameterization of the DFTB3 method for Br, Ca, Cl, F, I, K, and Na in organic and biological systems, J. Chem. Theory Comput. 11 (1) (2015 Jan 13) 332–342.
[34] S.T. Tan, B.J. Chen, X.W. Sun, W.J. Fan, H.S. Kwok, X.H. Zhang, S.J. Chua, Blueshift of optical band gap in ZnO thin films grown by metal-organic chemical-vapor deposition, J. Appl. Phys. 98 (1) (2005 Jul 1), 013505.
[35] Takahashi K., Yoshikawa A., Sandhu A. Wide bandgap semiconductors: fundamental properties and modern photonic and electronic devices. 2007.
[36] X. Wu, Z. Wei, Q. Liu, T. Pang, G. Wu, Structure and bonding in quaternary AgAuPdPt clusters, J. Alloys Compd. 687 (2016 Dec 5) 115–120.
[37] T.C. Yu, R.F. Brebrick, The Hg-Cd-Zn-Te phase diagram, J. Phase Equilib. 13 (5) (1992 Oct 1) 476–496.
[38] C. Lu, Y. Cheng, Q. Pan, X. Tao, B. Yang, G. Ye, One-dimensional growth of zinc crystals on a liquid surface, Sci. Rep. 6 (1) (2016 Jan 29) 1–7.
[39] M. Kurban, O.B. Malcıoğlu, Ş. Erkoç, Structural and thermal properties of Cd–Zn–Te ternary nanoparticles: Molecular-dynamics simulations, Chem. Phys. 464 (2016 Jan 13) 40–45.
[40] H. Kurban, M. Dalkilic, S. Temiz, M. Kurban, Tailoring the structural properties and electronic structure of anatase, brookite and rutile phase TiO2 nanoparticles: DFTB calculations, Comput. Mater. Sci. 183 (2020 Oct 1), 109843.
[41] S. Boggs Jr, Petrology of Sedimentary Rocks, 2nd edition, University of Oregon, Cambridge University Press, 2006.
[42] A. Pandey, H. Scherich, D.A. Drabold, Density functional theory model of amorphous zinc oxide (a-ZnO) and a-X0. 375Z0. 625O (X= Al, Ga and In), J. Non Cryst. Solids 455 (2017 Jan 1) 98–101.
[43] T. Eguchi, H. Inoue, A. Masuno, K. Kita, F. Utsuno, Oxygen close-packed structure in amorphous indium zinc oxide thin films, Inorg. Chem. 49 (18) (2010 Sep 20) 8298–8304.
[44] H.X. Deng, S.H. Wei, S.S. Li, J. Li, A. Walsh, Electronic origin of the conductivity imbalance between covalent and ionic amorphous semiconductors, Phys. Rev. B 87 (12) (2013 Mar 21), 125203.
[45] A. Walsh, J.L. Da Silva, S.H. Wei, Interplay between order and disorder in the high performance of amorphous transparent conducting oxides, Chem. Mater. 21 (21) (2009 Nov 10) 5119–5124.
[46] S.M. Hosseini, I.A. Sarsari, P. Kameli, H. Salamati, Effect of Ag doping on structural, optical, and photocatalytic properties of ZnO nanoparticles, J. Alloys Compd. 640 (2015 Aug 15) 408–415.
[47] C.J. Chang, T.L. Yang, Y.C. Weng, Synthesis and characterization of Cr-doped ZnO nanorod-array photocatalysts with improved activity, J. Solid State Chem. 214 (2014 Jun 1) 101–107.
[48] N. Sharma, R.P. Singh, V. Sharma, Effect of silver dopant on structural and optical properties of ZnO nanoparticles, Appl. Phys. A 125 (5) (2019 May 1) 326.
[49] R.P. Singh, I.S. Hudiara, S. Panday, S.B. Rana, Effect of Ni doping on structural, optical, and magnetic properties of Fe-Doped ZnO nanoparticles, J. Supercond. Novel Magn. 28 (12) (2015 Dec 1) 3685–3691.
[50] Y. Liu, Q.Y. Hou, H.P. Xu, L.M. Li, Y. Zhang, First-principles study of the effect of heavy Ni doping on the electronic structure and absorption spectrum of wurtzite ZnO, Physica B 407 (13) (2012 Jul 1) 2359–2364.
[51] X.L. Zhang, K.S. Hui, K.N. Hui, High photo-responsivity ZnO UV detectors fabricated by RF reactive sputtering, Mater. Res. Bull. 48 (2) (2013 Feb 1) 305–309.
[52] Y. Jin, Y. Ren, M. Cao, Z. Ye, Doped colloidal ZnO nanocrystals, J. Nanomater. (2012 Jan 1) 2012.